Deep-Sea Research II 58 (2011) 2524–2532

Contents lists available at ScienceDirect

Deep-Sea Research II

journal homepage: www.elsevier.com/locate/dsr2

Variations of Winter Water properties and sea ice along the Greenwich meridian on decadal time scales

A. Behrendt, E. Fahrbach*, M. Hoppema, G. Rohardt, O. Boebel, O. Klatt, A. Wisotzki, H. Witte

Alfred-Wegener-Institut für Polar- und Meeresforschung in der Helmholtz-Gemeinschaft, Bremerhaven, Germany

ARTICLE INFO

Available online 13 July 2011

Keywords:
Water masses
Winter Water
Sea ice
Variations
Polynya
Southern Ocean
Greenwich meridian

ABSTRACT

Sea–ice ocean interaction processes are of significant influence on the water mass formation in the Weddell gyre. On the basis of data obtained between 1984 and 2008 from eight repeat hydrographic sections, moored instruments and profiling floats in the Weddell gyre on the Greenwich meridian – almost all of them collected with R.V. *Polarstern* – we identified variations in the properties of the Winter Water and the sea ice draft. In the Winter Water the salinity was relatively low throughout the 1990s (with a minimum in 1992) and a maximum was observed in 2003. Observations of sea ice draft by moored upward looking sonars are available from 1996 onwards. In the southern part of the transect they display variations on a decadal time scale with a minimum in sea-ice thickness in 1998 and an increase since then. Salinity variations in the Winter Water layer cannot be explained only by variations in sea-ice formation and variable entrainment of underlying Warm Deep Water, but lateral advection of water and sea ice needs to be taken into account as well. Potential sources are melt water from the ice shelves in the western Weddell Sea or transport of water of low salinity entering the Weddell gyre from the east. Accompanying variations of the properties of Warm Deep Water are discussed in detail in a companion paper (Fahrbach et al., 2011).

1. Introduction

The Weddell Sea is one of the main regions of ventilated water production in the Southern Ocean (Orsi et al., 1999). These waters are transferred into the Antarctic circumpolar water belt and from there they spread equatorwards as part of the lower limb of the global thermohaline circulation (Heywood and Stevens, 2007). This renders the processes occurring in the Weddell Sea some relevance to the global climate.

Dense bottom and deep waters are generated over the shelves of the Weddell Sea (Foster et al., 1987; Foldvik et al., 2004; Nicholls et al., 2009), where salt rejection following sea ice formation leads to the dense surface water component of the nascent deep and bottom waters. The other main mixing ingredient is the Circumpolar Deep Water (locally known as Warm Deep Water), which has been transferred into the Weddell Sea from the Antarctic Circumpolar Current to the north. Apart from this saline mode of ventilated deepwater production, a thermal mode exists which is associated with open ocean deep convection (Gordon, 1991). During the last three decades the saline mode was active; only in the mid-1970s the thermal mode is known to have been dominant, the large Weddell polynya being its expression (Gordon, 1978). Smaller open ocean polynyas occur in the Weddell gyre as transients (Comiso and Gordon, 1996), and they testify of smaller convection events.

The very name "thermal mode" strongly emphasizes the role of temperature as a main factor during deepwater formation. However, the salinity level of the surface layer is an essential co-factor for the overturning potential. The thermal mode can only become active if the surface layer contains sufficient salt. In the Weddell gyre the seasonally varying formation and melting of sea ice is a main factor of variation of surface layer salinity. However, upwelling and entrainment of salt-rich deep water plays a significant role as well (Gordon and Huber, 1990). Variability of one or the other may decisively condition the salinity of the surface layer, which in turn may destabilize the stratification. It should be realized that the local stratification is relatively weak and thus surface layer processes could easily induce convective overturning.

Evidence is accumulating that certain modes of climate variability in the Southern Ocean, of which the Southern Annular Mode (SAM) (Hall and Visbeck, 2002; Thompson and Solomon, 2002) is the most important, are affecting the Weddell gyre. Kerr et al. (2009) suggested a correlation between the SAM and Weddell Sea Bottom Water. Gordon et al. (2007) even suggested a relationship between the changing Southern Annular Mode and the occurrence of the Weddell polynya. Thus, the salinity trends should also be considered in the light of ocean-wide mechanisms. Long-term trends in surface water salinity, resulting in a decreasing salinity of the bottom water in the Indian sector of the Southern Ocean, have been observed (Rintoul, 2007), which was also found by Aoki et al. (2005). Boyer et al. (2005)

* Corresponding author. Tel.: +49 471 4831 1820; fax: +49 471 4831 1797.
E-mail address: Eberhard.Fahrbach@awi.de (E. Fahrbach).

0967-0645/$ - see front matter © 2011 Elsevier Ltd. All rights reserved.
doi:10.1016/j.dsr2.2011.07.001

calculated, based on quality controlled data, significant trends of salinity in all ocean basins, with freshening in the Weddell and Ross Seas. Hellmer et al. (2009) show that surface water salinity anomalies move through the Weddell gyre from the east to the west, emphasizing the role of advection in the salinity issue. Similarly, Park et al. (1998) described the advection of freshwater from the Weddell basin to the Enderby Basin to the east. Jacobs et al. (2002) reported the decrease of salinity in the shelf waters of the Ross Sea, which causes the bottom waters originating from that region to become fresher. Freshening of the northwestern Weddell Sea continental shelf was detected by Hellmer et al. (2010).

On average over the Southern Ocean, the salinity of the surface layer exhibits a strong seasonal cycle with an increase from March to October and a decrease from November to February (Dong et al., 2009). To determine the salinity budget one has to include the major terms advection, diffusion, upwelling/entrainment, and freshwater fluxes. According to Dong et al. (2009), advection and entrainment are the major factors, while freshwater fluxes contribute much less. Locally this may be different, though.

Here we present data of winter surface layer salinity which span a time period of more than 20 years based on traditional hydrographic (Fahrbach et al., 2007) and recent float data. For the purpose of comparing all those data collected in different seasons, the actually observed salinities had to be adjusted to obtain apparent winter values. In addition, ice draft data from moored upward looking sonar instruments are presented for investigating the interactions between the water and the sea ice. These data may give clues as to the probability of a switch from the current saline mode to the thermal mode and thus to the possible formation of a large, non-transient polynya. Since the time lag from section to section varies from one to eight years a quantitative analysis is not feasible. Still, consistent variations on multiannual to decadal time scales suggest correlations between relevant processes which help to understand the functioning of the Weddell system.

2. The data

Hydrographic data of all but one cruise (AJAX in 1984) were collected during cruises with the ice breaker R.V. *Polarstern* between 1992 and 2008. Here we concentrate on the data from the Greenwich meridian (Fig. 1). For details we refer to the companion paper (Fahrbach et al., 2011).

Data sets from the Greenwich meridian (southern part of WOCE section A12) include the following:

AJAX (leg 2) 16–29 January 1984
ANT-X/4 5–19 June 1992
ANT-XIII/4 12–23 April 1996
ANT-XV/4 29 April–16 May 1998
ANT-XVIII/3 20 December 2000–2 January 2001
ANT-XX/2 30 November–19 December 2002
ANT-XXII/3 31 January–09 February 2005
ANT-XXIV/3 19 February–12 March 2008

Temperature and salinity were collected using a CTD instrument (conductivity, temperature, depth). Since 2000 a Seabird SBE 911plus CTD has been used. Salinities are reported on the Practical Salinity Scale (PSS78). Data of all cruises are accurate to at least 0.003 °C in temperature, 2 dB in pressure and 0.003 in salinity.

Moorings were maintained at the Greenwich meridian between 69.4°S and 57°S from 1996 to 2008 (Fig. 1). The upper end of the moorings had to be placed with sufficient distance to the surface to reduce the risk of damage by passing icebergs and the disturbance by surface gravity waves. Thus instruments hardly ever record data in the Winter-Water layer (see Fig. 6 of Fahrbach et al., 2011). Therefore

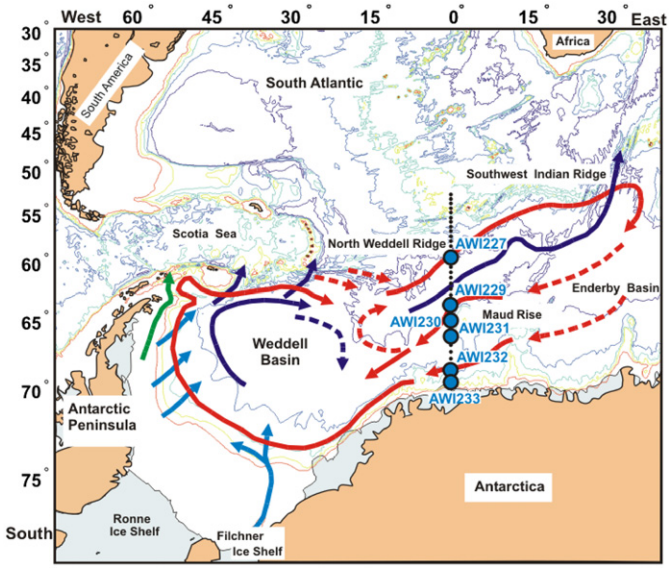

Fig. 1. Map of the Atlantic sector of the Southern Ocean including the generalized circulation of the Weddell gyre, the location of the section at the Greenwich meridian and of the moorings AWI 227, AWI 229, AWI 230, AWI 231, AWI 232 and AWI 233 on which upward looking sonars were deployed. Red arrows indicate circulation of Circumpolar (Warm) Deep Water, light blue arrows sinking water masses along the continental slope. Dark blue arrows depict deep and bottom water circulation and water masses leaving the basin. The green arrow indicates shelf water leaving the western Weddell Sea. Dashed arrows indicate either transient currents or eddy exchanges.

comprehensive time series of Winter-Water properties are not available. Still some hints as to the seasonal to interannual variability can be deduced. Apart from current meters and temperature sensors, they carried upward looking sonars (ULS) for measuring sea-ice draft (Fahrbach and De Baar, 2010), data of which are presented here. The instruments measure the subsurface portion of sea ice, i.e., the ice draft (Fig. 2). ULS transmit ultrasonic sound waves from about 150 m depth towards the ice bottom and measure the time the sound signal needs to travel to the reflecting ice/water interface and back. With the known sound velocity the measured time period can be converted into a distance. Subtracting this distance from the instrument depth yields the sea-ice draft. When profiling open water, e.g., leads between ice floes, the measured sonar distance equals the ULS depth. As the sea-ice bottom is not a perfect reflector for sound waves (Melling, 1998), strong transducers are needed.

The instruments used are ES-300 series ULS, manufactured by Christian Michelsen Research (CMR) in Norway. They use ceramic transducers that transmit 300 kHz signals in bursts of four pulses. Depending on the battery capacity, the bursts are transmitted in intervals of 2–15 min. In this way, a ULS can record more than a hundred thousand data cycles during deployment periods of several years. A pressure sensor measures with an accuracy of 0.05% for determining the instrument depth. In addition, an inclinometer measures the instrument tilt angle with an accuracy of 1°, and the water temperature is measured by a thermistor. The travel times of the echoes are recorded and stored as 8- or 16-bit digitized voltage values.

The instrument is attached to the upper end of an oceanographic mooring at around 150 m depth (Fig. 2). At this depth, the opening angle of the acoustic beam of 2.5° results in a surface window (footprint) of approximately 6–7 m in diameter. This footprint always contains ice of different thickness. As the ULS detects the echo signals that arrive first, the measured ice draft is always represented by the deepest protruding points of the ice underside. Ice draft is therefore systematically overestimated. This bias is hard to quantify, but several ULS studies estimated it to be 10–11.5% (e.g., Strass, 1998). As the

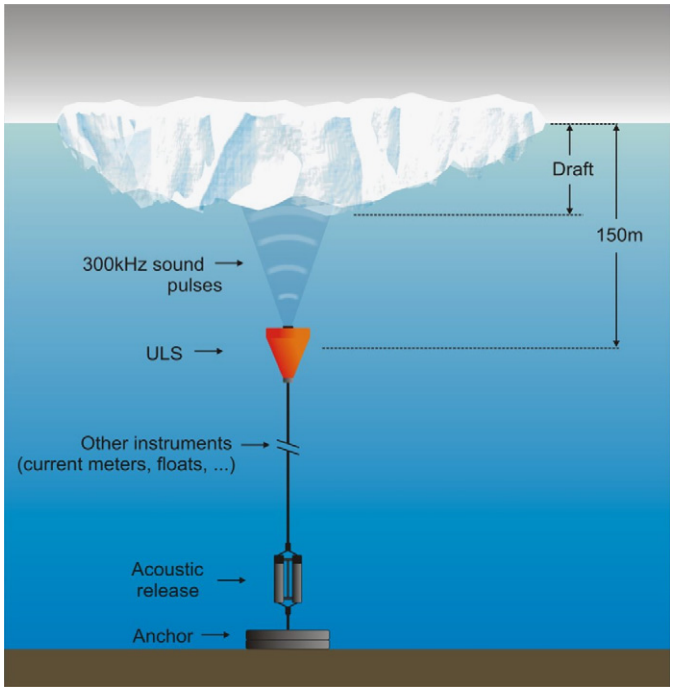

Fig. 2. Schematic representation of a mooring with an upward looking sonar (ULS) as deployed along the Greenwich meridian. The instrument transmits acoustic pulses which are reflected at the sea-ice underside. The transit time is used to calculate the distance from which the ice draft is derived.

ambient water pressure is influenced by the atmospheric pressure, the ULS pressure readings are corrected with reanalysis data from the European Centre for Medium-Range Weather Forecasts (ECMWF). Another error source is the sound velocity, which is not uniform in the water column above the ULS. Changes in sound speed can result in distance errors of more than 20 cm and cannot be ignored. Temperature and salinity profiles, from which the sound speed may be calculated, are not available on an hourly basis. The processing algorithm used at AWI enables the operator to visually detect open water areas, to assess the draft data and manually correct the reference level of open water (zero draft). A comprehensive discussion of error sources and zero level correction can be found by Melling et al. (1995). Errors due to sound speed variations are accounted for by the correction during the data processing. However, this way of correcting the data is subjective and depends to some extent on the experience of the data analyst. To reduce this "human error", daily and monthly mean values of sea-ice draft were calculated from two draft files processed by different operators and were then averaged. The accuracy of draft values processed by an earlier version of the algorithm was estimated at 4 cm (Strass, 1998). Values of comparable ULS deployed in the Arctic are typically accurate within ± 0.1 m (Melling and Riedel, 1995). We adapt this estimate as the more realistic one. Under consideration of the assumed accuracy of the ice-draft measurements, we do not transfer draft into thickness but take the variations in draft as equivalent to the ones in thickness.

Results of earlier draft measurements were presented by Strass and Fahrbach (1998), and were also used for ice volume flux estimations (Drinkwater et al., 2001; Harms et al., 2001). The measurements presented here are concentrated on the Greenwich meridian and started in 1996 with ULS on six positions (Fig. 1). The ULS instruments were recovered and redeployed by *Polarstern* for measurement periods of 2–3 years during the whole 12-year period from 1996 to 2008, except for AWI-227 and AWI-230 which were deployed only until 2000 and 2002, respectively. The loss rate due to damaged instruments or lost moorings was about one-third, and the data rate of the remaining instruments was 78%.

Since 1999, AWI deployed more than 130 Argo floats within the Weddell gyre. Delayed mode quality control was applied according to Argo standard (Owens and Wong, 2009), comparing float data to high quality reference CTD data (climatology). These comparisons were made on deep isotherms and assumed that the temperature sensor of the float is stable and that salinity on deep isotherms was steady and uniform. The accuracy of the float data is better than 0.01 °C in temperature and 0.01 in salinity (Argo standard). We present data of float WMO 7900093; it was deployed in March 2005 and was active until December 2008 (Fig. 3). An onboard "Ice Sensing Algorithm" (ISA) prevented the float from surfacing in ice covered waters and hence protected it from being destroyed or damaged by the ice (Klatt et al., 2007). Since 2005 under-ice profiles, were stored successfully throughout winter and transmitted during subsequent summer seasons. In this way, float WMO 7900093 performed 135 profiles covering three winter seasons. Owing to not resolved technical problems of different origin, the under-ice data are still rare.

To calculate the mean properties of the Winter-Water layer, the data set was gridded with a distance of 1 m in the vertical and 1 km in the horizontal. The uncertainty of the mean values is determined by the horizontal and vertical variations along each transect. With a correlation length of 50 km horizontally (i.e., more than the station distance) and 10 m vertically, we have about 250–500 independent samples per water mass. On this basis the uncertainties for the mean potential temperatures and salinities were calculated from the standard deviation.

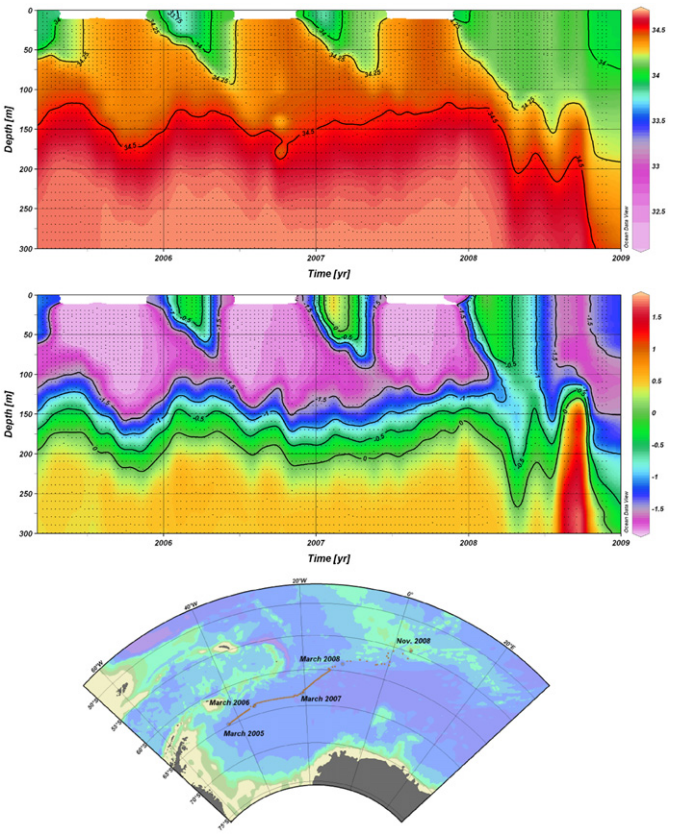

Fig. 3. Isopleth diagrams of salinity (top) and in-situ temperature (middle) of the upper layers in the Weddell Sea from vertically profiling float WMO 7900093. The drift track (bottom) is depicted by dots 10 days apart at each location at which the float came to the surface. Under the sea ice the tracks were linearly interpolated east and west of 40°W, 30°W and east of 20°W. Contour plots were created with ODV (Schlitzer, 2010).

We calculated temperature and salinity time series using all section data at the Greenwich meridian from 1984 to 2008. Computing methods were similar to those described by Fahrbach et al. (2011). For investigating the large-scale picture, cross-basin averages of potential temperature and salinity were computed in order to diminish the effect of small to meso-scale features on the detection of low period changes of water mass properties. We split the calculation in the northern and southern part of the gyre and obtained consistent results (Fig. 10), which evidenced that the large scale patterns are independent on the averaging area.

3. Results

3.1. Near surface water mass properties

Just like the deep and bottom waters, the surface layer ultimately derives from the Warm Deep Water (WDW) (Gordon and Huber, 1990; Fahrbach et al., 1994). The dissimilar characteristics of WDW and surface water are brought about by upper ocean processes, such as ice formation and melting, precipitation and evaporation, biological activity and air–sea exchange. Water masses in the upper layers are separated from the WDW by a sharp permanent pycnocline. The upper layer consists of Antarctic Surface Water (AASW) and Winter Water (WW). Their temperatures range from the freezing point in winter to a few degrees above that in summer. As its name implies, the Winter Water fills up the surface layer in that particular time of the year and its temperature is very close to the freezing point. However, it is also observed during the rest of the year: in spring and early summer, the upper part of the surface layer is heated up (Fig. 3). Due to the stable stratification, the lower part of the winter surface layer cannot be reached by the heating from the surface and so it keeps its near-freezing temperature; it is thus a remnant of the Winter Water. Still, some temperature increase may occur, due to WDW entrainment or diffusion from below in the course of the summer season. At the Greenwich meridian section, the WW is visible at depths of 50–120 m all across the gyre. The temperature minimum of the WW occurs as far north as the Polar Front, but outside the Weddell gyre its temperature is higher than inside. As to the deep water masses, we refer to the companion paper (Fahrbach et al., 2011).

3.2. The mean sea-ice draft

The ice conditions in the Weddell gyre area, in particular on the Greenwich meridian, are subject to an intensive annual cycle (Zwally et al., 2008). Whereas in winter sea ice (with a concentration of more than 15%) reaches up to 55°S, in summer it melts away completely up to the coast and ice cover remains only in the southern and western Weddell Sea (Fig. 4).

The mean sea-ice draft along the Greenwich meridian is relatively constant across the gyre and only increases towards the coast (Fig. 5 and Table 1). In the north at 59°S (AWI 227), the mean sea-ice draft during the period when ice is present amounts to 0.57 m with a mode of 0.5 m, while the ice cover lasts 228 days on average. To the south the mean draft is 0.64 m north of Maud Rise at about 64°S (AWI 229) during a period of 241 days. Around Maud Rise at 66–66.5°S (AWI 230 and AWI 231) similar mean drafts of 0.67 and 0.65 m and periods of ice cover of 248 and 246 days are observed. Towards the coast at 69°S (AWI 232) and 69.4°S (AWI 233), the ice draft is much higher with 1.7 and 2.4 m, and durations of 320 and 359 days, respectively. The mode (i.e., the most frequently observed value) remains at 0.4–0.5 m along the entire transect. The statistical properties of the sea-ice distribution are displayed as probability distributions in Fig. 5.

3.3. Variations of the near-surface water masses

Water masses in the surface layer are directly involved in ocean–ice–atmosphere interactions. To quantify decadal-scale variations of the near-surface properties using CTD transects, the pronounced annual cycle has to be taken into account, since the measurements were conducted in different seasons or different phases of the season: in spite of the fact that most cruises are in the Antarctic summer season, early or late summer makes a big difference with regard to the annual cycle. To eliminate the seasonal aliasing of our estimates of the properties of the Winter Water, we applied a method whereby the initial winter properties for the sections were derived with the help of winter data obtained by profiling floats. The isopleth diagrams of temperature and salinity from float WMO 7900093, drifting in the Weddell Sea between 2005 and 2009, illustrate the seasonal evolution of the Winter Water layer (Fig. 3). In March/April, winter convection erodes the summer layer within about a month and reaches the

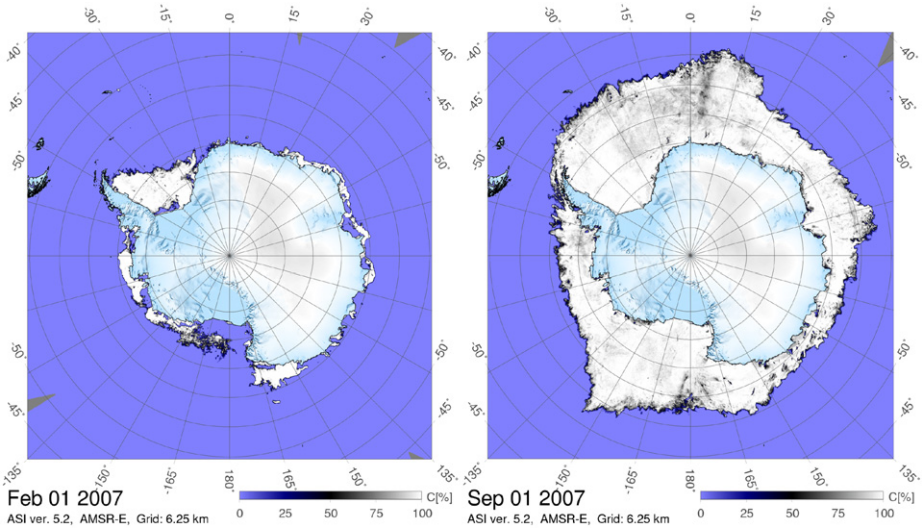

Fig. 4. Concentration of sea ice around Antarctica for February and September 2007. The Weddell gyre is situated at the top of the pictures, east of the outstanding Antarctic Peninsula. Data from www.seaice.de (Spreen et al., 2008).

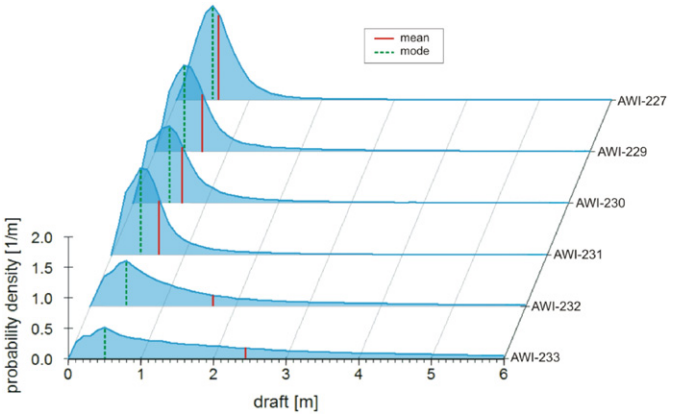

Fig. 5. Probability density distribution of sea-ice draft observed from 1996 to 2008 with upward looking sonars at the Greenwich meridian between 59°S and 69.4°S for moorings AWI 227, AWI 229, AWI 230, AWI 231, AWI 232 and AWI 233. For positions see Fig. 1. The open water period in summer was removed before the calculation. The density functions are shown for each ULS. Bold red lines: mean values, dashed green lines: modal values. (For interpretation of the references to color in this figure legend, the reader is referred to the web version of this article.)

Table 1
Mean sea-ice properties from moored upward looking sonars along the Greenwich meridian.

Mooring	Latitude	Record duration	Mean (m)	Mode (m)	Season's duration (days)
227	−59.07	568	0.57	0.5	228
229	−63.95	1529	0.64	0.4	241
230	−66	472	0.67	0.5	248
231	−66.5	1706	0.65	0.4	246
232	−68.98	2365	1.69	0.5	320
233	−69.38	973	2.43	0.5	359

WW from the previous year which is slightly warmer than freezing temperature. With ongoing convection the new WW layer deepens and increases slightly in salinity until August/September, when the ice cover is fully established. After that, with decreasing intensity of convection, upward motion in the Weddell gyre becomes dominant, shifting the lower boundary of WW upwards. In December after the melt-back of the sea ice, a warm and low saline summer layer is formed at the surface. The WW gradually warms and the temperature minimum becomes less saline. In this particular case of observations from float WMO 7900093, apparent differences from year to year were to some extent due to the northeastward propagation of the float in the gyre (Fig. 3 bottom), thus crossing changing surface regimes. The basis for adjusting the measured salinity to the WW value is the fact that the observed salinity of WW in winter is well represented in the θ/S diagram by the extrapolation of a line linking the WDW maximum and the θ/S point at −1 °C to the freezing temperature. This empirical knowledge was confirmed by data from floats in the vicinity of the Greenwich meridian. However since most of the floats were deployed in summer along the Greenwich meridian only a few floats provided winter data in that area. The derived relation was applied to the CTD profiles for obtaining the previous winter values from the actually measured ones (Fig. 6).

WW salinity was high in 1984 and decreased to an absolute minimum in 1992 (Fig. 7). Obviously, we are not able to exclude intensive interannual variations in this time period. From 1992 onwards there was a positive trend until 2003. From then on the WW freshened again. The unadjusted values differ significantly from

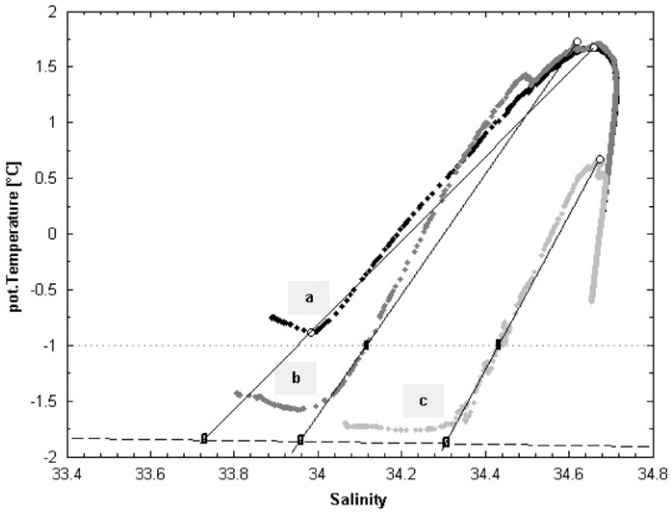

Fig. 6. Potential temperature/salinity diagrams in the transition zone from northern Weddell gyre to the Antarctic Circumpolar Current on the Greenwich meridian at (a) 54°S, (b) 55°S and (c) 57.5°S measured in 2002 during cruise ANT-XX/2. Straight lines are drawn from the temperature maximum to the salinity at −1 °C, or at the temperature minimum (as for curve (a)). The extrapolation of this line cutting the temperature/salinity line of the freezing point represents the Winter Water salinity. Such relationships were derived from potential temperature/salinity diagrams of profiling floats for obtaining the salinity at freezing point in cases when the Winter Water was only sampled during non-winter conditions.

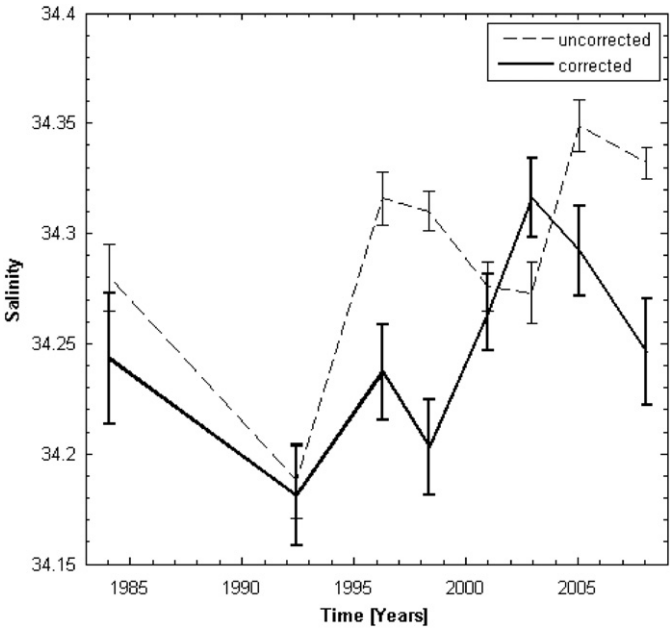

Fig. 7. Time series of the mean salinity of the Winter Water derived from the all-section data along the Greenwich meridian. The dashed line represent measured values, the solid line values adjusted to winter conditions according to the correction procedure shown in Fig. 6. The error bars were calculated as the error of the mean values of independent samples.

the adjusted ones, but also in the unadjusted data a significant increase occurred from the early 1990s to the mid-2000s. We cannot exclude some effect by aliasing of seasonal to interannual fluctuations as a contribution to the observed variation; however, the time series from the moored instruments displayed by Fahrbach et al. (2011) suggest that the variations of the Warm Deep Water are well captured by the CTD sections. We use this as an indicator that the general structure of the multi-annual WW variations are captured by the sections as well.

The salinity of the WW plays a significant role in the stability of the upper water column, as a higher WW salinity will ease convective overturning. The stability, defined here as the potential density difference between the WDW and the WW, decreased from the early 1990s until 2003 (Fig. 8). However, before becoming unstable after 2003 with ensuing deep overturning convection and the possible formation of a large Weddell polynya, the stability of the water column increased again in recent years in consequence of the freshening of WW.

3.4. Variations of the sea-ice draft

Variations of the sea-ice draft are shown in Fig. 9. It has to be noted that the record lengths at the different moorings differ significantly (Table 1). Here, we concentrate on the multi-annual variations. Different regimes can be distinguished in the northern and southern part of the observation area (Fig. 9). In the north, bi-annual fluctuations prevail and no clear decadal signal can be identified. In the south, sea-ice draft decreases from 1996 to 1999 and increases afterwards until the end of the record in 2008 with superimposed bi-annual fluctuations.

4. Discussion

Three processes are potentially responsible for water mass properties variations of the Winter Water in the Weddell gyre:

- variation of the interactions with the underlying WDW,
- variations of sea-ice formation and
- variations of external freshwater sources.

4.1. Variations of the interactions with the underlaying WDW

The variations of the deep water mass properties were discussed in detail in the companion paper (Fahrbach et al., 2011). Briefly, the temperature and salinity as well as the layer thickness of WDW were subject to a decadal fluctuation. The average of the WDW temperature and salinity over the full transect from 56°S to 69.4°S had maxima in 1998 and minima in 2005. The maxima and minima in

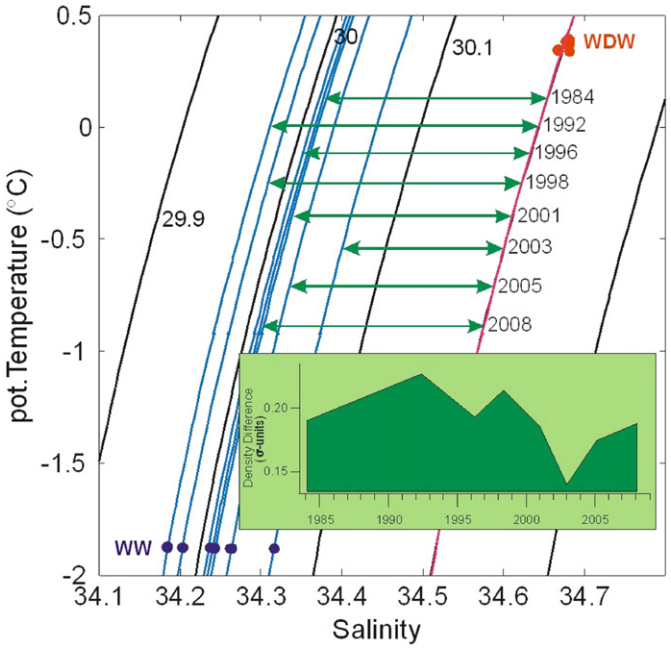

Fig. 8. Variation of the potential density difference between the Winter Water and the Warm Deep Water (WDW) displayed in a θ/S diagram for the CTD transects from 1984 to 2008. The green arrows indicate the distance between the isopycnals of WDW and the WW of the individual transect. The green inlay displays the potential density difference as time series.

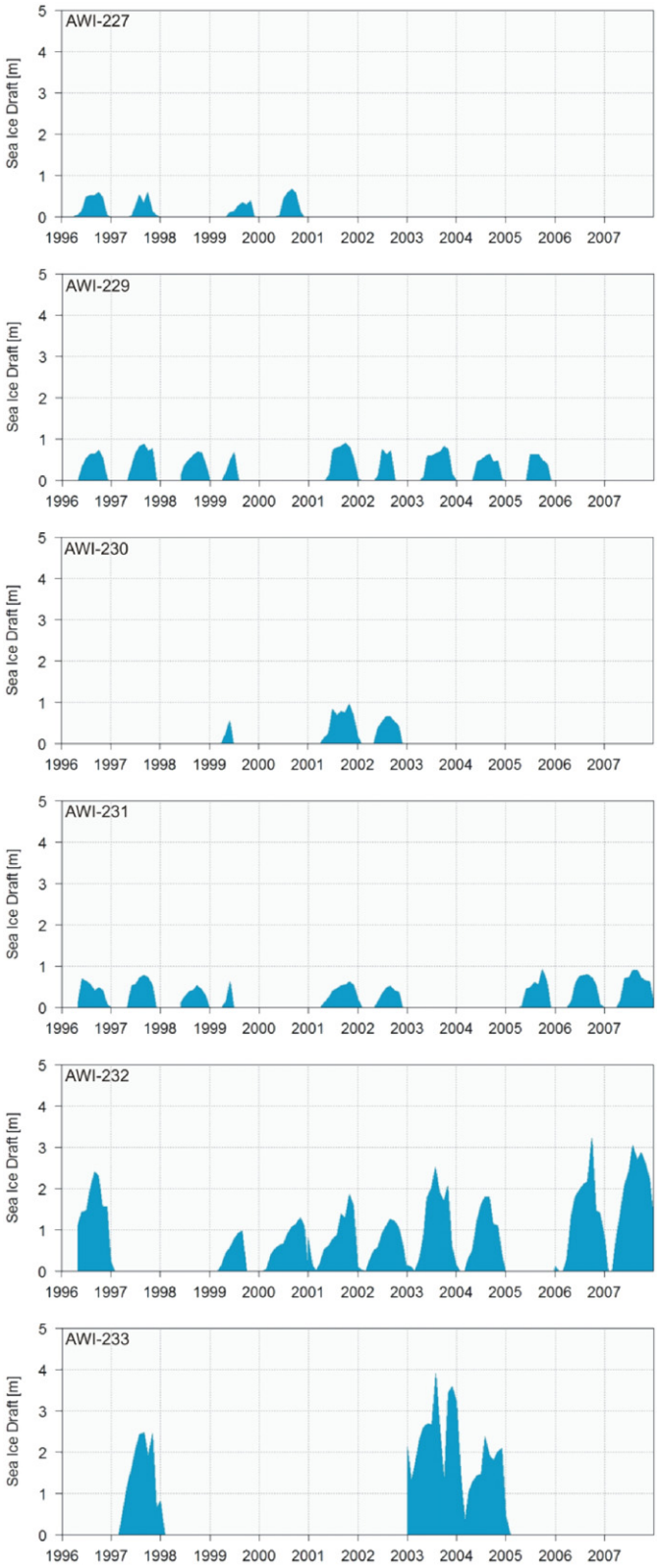

Fig. 9. Time series of ice draft measured with upward looking sonars at the Greenwich meridian on moorings AWI 227, AWI 229, AWI 230, AWI 231, AWI 232 and AWI 233. For positions see Fig. 1.

the WDW layer thickness preceded those of average temperature and salinity by about 2–4 years.

The increased inflow of WDW, evidenced by the increasing layer thickness, with ensuing erosion of the WDW layer would tend to increase the salinity of the WW due to the elevated entrainment of saline WDW into the WW. However, this can only partly explain the observed salinity variations (Fig. 7). The WW salinity has a minimum in 1992 during the first inflow event of WDW and a maximum in 2003. The upper boundary of the WDW decreased from 142 to 127 m from 1992 to 1996 (Fig. 10B). After a period of almost constant layer thickness (Fig. 10A), further WDW warming took place from 2005 to 2008 which leads to the largest WDW layer thickness (Fig. 10A) and the shallowest boundary of WDW of the entire record (Fig. 10B). At the same time the WW salinity decreased again (Fig. 7). The two phases of decreasing WW layer thickness and first increasing and then decreasing salinity suggest a different origin of the causes.

Assuming an upwelling rate at and near the Greenwich meridian of 30–45 m/year (Gordon and Huber, 1990; Hoppema et al., 1995), the upper 25 m of WDW are entrained into the WW layer within 1 year. Under steady conditions this lost WDW must be resupplied to the gyre and the salinity gain of WW must be compensated by freshwater gain of about 0.3 m.

During the first phase from 1992 to 1996, WW salinity increases from 34.18 to 34.23 (Fig. 7). This can be explained by the erosion of a 15 m layer of the WDW from 142 to 127 m as observed during that period (Fig. 10B). In the next phase from 1998 to 2003 WW salinity increases further from 34.21 to 34.32, but the depth of the WW layer remains almost constant. Here, the variation of the sea-ice thickness increasing from 1998 to 2003 (Fig. 9) has to be taken into account.

Since the observed decadal variation of the sea-ice draft is only visible in the southern mooring AWI 232, we display as well the variations of the WDW and WW layer thickness of the southern limb of the gyre (Fig. 10C and D) as average between 60°S and 69.4°S. It appears that the variations of the southern limb and the whole transect are rather consistent.

It is worthwhile noting that changes in the WW closely interact with and have consequences for the WDW, e.g., lower salinity in the WW leads to more stratification and thus less convective overturning. This in turn will tend to reduce the vertical transport of WDW into the WW, a positive feedback to salinity reduction of the WW and a reduction of heat transport to the surface.

4.2. Variations of the sea-ice formation

Variations of the sea-ice formation can be either induced by atmospheric forcing including heat exchange and wind driven divergences or convergences, or by the heat supply from below,

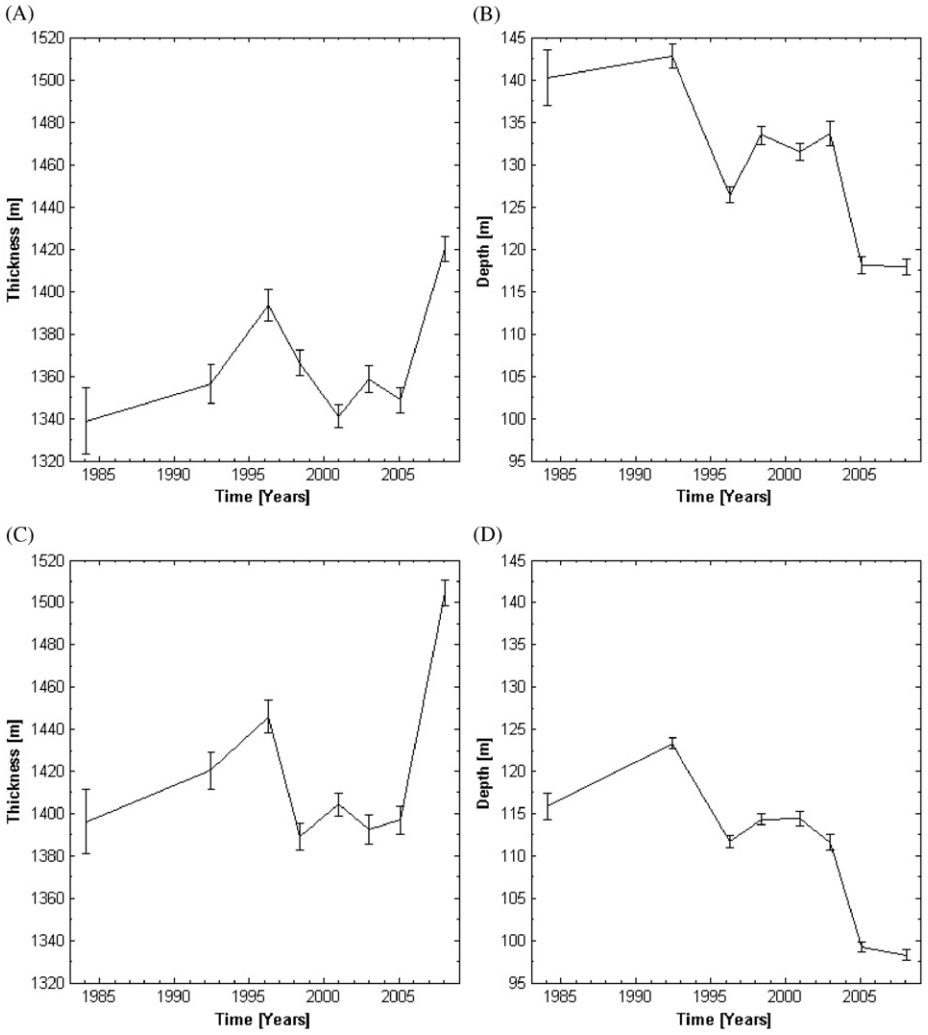

Fig. 10. Time series of properties of the Warm Deep Water as defined by neutral density over the section along the Greenwich meridian as averages over the full transect from 56°S to 69.4°S (A) and (B) and over the southern gyre limb from 60° to 69.4°S (C) and (D). The thickness of the WDW layer is displayed in (A) and (C) and the depth of upper limit of the WDW (at $\gamma^n = 28.0$ kg/m^3) in (B) and (D).

i.e., the WDW. Here we focus on the effect of variations related to the WDW variations.

The variation of the sea-ice thickness on the southern part of the transect as displayed at mooring AWI 232 (Fig. 9) correlates to the thickness of the WDW in the southern limb of the gyre (Fig. 10C and D). When the sea-ice thickness decreased from 1996 to 1999, the WDW layer thickness decreased as well with subsequent increase which is most intense for both of them from 2005 to 2008. The boundary between WDW and WW follows the pattern of being deep when the WDW layer is thin and shallow when the WDW layer is thick. In consequence, the WW layer is shallow when the sea ice is thick. This seems to be contradictory, since we expect a larger heat transport upwards during periods of a shallow WW layer which then would act to reduce sea ice formation.

The correlation of decreasing WW layer thickness and increasing sea-ice thickness suggests that the latter is determined to a lesser extent by heat transports from the ocean (in particular from the WDW) than by the dynamic effects related to the ice transport. The variations of the wind and current system as displayed in the companion paper (Fahrbach et al., 2011) support this notion. From 1996 onwards, i.e., during the period of sea-ice thickness measurements, the westward current measured by moored instruments in the southern gyre limb increased from a minimum in 1998, correlating to the increase in sea-ice thickness. The increasing current intensity is related to the increasing easterly winds in the south (Fahrbach et al., 2011) and the decreasing westerlies in the north. We speculate that increasing westward drift leads to a convergence in the area of the Greenwich meridian inducing ice draft and salinity increase since both the newly formed ice and the released salt are converging.

A sea-ice thickness increase of 0.45 m over the time period from 1998 to 2003 is able to explain the WW salinity increase displayed for this period in Fig. 7. This is consistent with the sea-ice thickness observations (Fig. 9). This increasing ice draft measured with the ULS is qualitatively in agreement with the long-term positive trend of sea-ice coverage in the Southern Ocean and Weddell Sea (Cavalieri and Parkinson, 2008). The third phase from 2003 to 2008 during which the WW salinity decreases can neither be explained by interaction with WDW since the WW is getting shallower again and sea ice is increasing in thickness. Therefore external freshwater inflow has to be considered.

4.3. Variations of external freshwater sources

A potential source of freshwater is iceberg melt. According to Silva et al. (2006) in the freshwater budget of the Weddell Sea, iceberg melt is more important than the precipitation minus evaporation term. There have been major break-off events at the Larsen Ice Shelf between 1995 and 2003 when significant amounts of freshwater were injected into the Weddell Sea (De Angelis and Skvarca, 2003; Rack and Rott, 2004). Depending on the area over which the freshwater from melting icebergs would spread, the salinity of the 140 m deep surface mixed layer may be reduced by between 0.1 and 0.01. The float track from the western Weddell Sea to the Greenwich meridian (Fig. 3) suggests that the meltwater should arrive about 3 years after the calving, i.e., in 1998 and 2006. The salinity minimum in 1998 would correspond well to the break-off of Larsen A in 1995 and the calving of Larsen B to the salinity decay from 2005 onwards. However, the ongoing salinity decrease to 2008 suggests that other freshwater sources contribute as well. A contribution might come from the variation of the freshwater input from the direct melt of ice shelf (e.g., Walkden et al., 2009) and is consistent with observations of freshening on the northwestern Weddell Sea as observed by Hellmer et al. (2010).

5. Conclusions

On the basis of CTD data obtained over a time period of 24 years, we discuss changes of the water mass properties and their causes. Due to the limited number of sections no clear-cut correlations can be calculated but qualitative relations can be inferred. The salinity of the Winter Water increased from 1992 to 2003 and has been decreasing since then. We argue that the three major salt sources for WW, which are salt release due to sea-ice formation, entrainment of salty WDW and advection either as melting icebergs or from outside the gyre, prevail during three different periods. This would also allow an opposing correlation of sea ice concentration and layer thickness, which is indicated in our data. During the first period from 1992 to 1996 when ice thickness observations were not yet available, increasing WW salinity is consistent with increasing WDW salinity and layer thickness suggesting dominating salt supply by entrainment of WDW. During the second period 1996 to 1999 (when sea-ice thickness observations were available), decreasing sea-ice thickness is consistent with WDW layer freshening. From 1999 onwards, sea-ice thickness increased inducing WW salinity increase until 2003. From 2003 to 2008 the WW salinity dropped significantly in spite of still increasing sea-ice thickness and entrainment of salt from WDW. We infer that during this time period, advection of low salinity water has been dominating. This is consistent with the travel time of melt water from the western ice shelves and points towards freshwater input as consequence of the decay of ice shelves.

The time series of the density differences between WW and WDW suggest that the potential for the formation of a large Weddell polynya increased until 2003 and decreases since then. Thus the chance of a polynya being formed in the near future is small.

Acknowledgments

This work is based on seven cruises of F.S. *Polarstern*. We are grateful to the masters and crews for their ongoing and most dedicated support. We want to thank the reviewers who provided us a great deal of very helpful suggestions. In particular they pushed us to split a previous version of the manuscript into two papers. We are not able to cite all those by name who contributed by their continuous efforts on land to keep *Polarstern* in operation. We are grateful to the Helmholtz-Gemeinschaft Deutscher Forschungszentren to support this research during the MARCOPOLI and PACES programs and to the Bundesministerium für Bildung und Forschung and its predecessors during the WOCE and the CLIVAR projects to maintain by ongoing support the long time series in the Weddell gyre.

References

Aoki, S., Rintoul, S.R., Ushio, S., Watanabe, S., Bindoff, N.L., 2005. Freshening of the Adélie Land Bottom Water near 140°E. Geophys. Res. Lett. 32, L23601. doi:10.1029/2005GL024246.

Boyer, T.P., Levitus, S., Antonov, J.I., Locarnini, R.A., Garcia, H.E., 2005. Linear trends in salinity for the World Ocean, 1955–1998. Geophys. Res. Lett. 32, L01604. doi:10.1029/2004GL021791.

Cavalieri, D.J., Parkinson, C.L., 2008. Antarctic sea ice variability and trends, 1979–2006. J. Geophys. Res. 113, C07004. doi:10.1029/2007JC004564.

Comiso, J.C., Gordon, A.L., 1996. Cosmonaut polynya in the Southern Ocean: structure and variability. J. Geophys. Res. 101, 18297–18313.

De Angelis, H., Skvarca, P., 2003. Glacier surge after ice shelf collapse. Science 299, 1560–1562.

Dong, S., Garzoli, S.L., Baringer, M., 2009. An assessment of the seasonal mixed layer salinity budget in the Southern Ocean. J. Geophys. Res. 114, C12001. doi:10.1029/2008JC005258.

Drinkwater, M.R., Liu, X., Harms, S., 2001. Combined satellite- and ULS-derived sea-ice flux in the Weddell Sea, Antarctica. Ann. Glaciol. 33, 125–132.

Fahrbach, E., De Baar, H. (Eds.), 2010. The Expedition of the Research Vessel "Polarstern" to the Antarctic in 2008 (ANT-XXIV/3). Berichte zur Polar- und Meeresforschung 606, AWI, Bremerhaven, 228 pp.

Fahrbach, E., Rohardt, G., Schröder, M., Strass, V., 1994. Transport and structure of the Weddell gyre. Ann. Geophys. 12, 840–855.
Fahrbach, E., Hoppema, M., Rohardt, G., Boebel, O., Klatt, O., Wisotzki, A., 2011. Warming of deep and abyssal water masses along the Greenwich meridian on decadal time scales: the Weddell gyre as a heat buffer. Deep-Sea Res. II 58, 2509–2523.
Fahrbach, E., Rohardt, G., Sieger, R., 2007. 25 Years of Polarstern Hydrography (1982–2007). WDC-MARE Reports 5, AWI, Bremerhaven and MARUM, Bremen, 94 pp.
Foldvik, A., Gammelsrød, T., Østerhus, S., Fahrbach, E., Rohardt, G., Schröder, M., Nicholls, K.W., Padman, L., Woodgate, R.A., 2004. Ice shelf water overflow and bottom water formation in the southern Weddell Sea. J. Geophys. Res. 109, C02015. doi:10.1029/2003JC002008.
Foster, T.D., Foldvik, A., Middleton, J.H., 1987. Mixing and bottom water formation in the shelf break region of the southern Weddell Sea. Deep-Sea Res. 34A, 1771–1794.
Gordon, A.L., 1978. Deep Antarctic convection west of Maud Rise. J. Phys. Oceanogr. 8, 600–612.
Gordon, A.L., 1991. Two stable modes of Southern Ocean winter stratification. In: Chu, P.C., Gascard, J.-C. (Eds.), Deep Convection and Deep Water Formation in the Oceans. Elsevier Science, Amsterdam, pp. 17–35.
Gordon, A.L., Huber, B.A., 1990. Southern Ocean winter mixed layer. J. Geophys. Res. 95, 11655–11672.
Gordon, A.L., Visbeck, M., Comiso, J.C., 2007. A possible link between the Weddell Polynya and the Southern Annular Mode. J. Clim. 20, 2558–2571.
Hall, A., Visbeck, M., 2002. Synchronous variability in the southern hemisphere atmosphere, sea ice, and ocean resulting from the annular mode. J. Clim. 15, 3043–3057.
Harms, S., Fahrbach, E., Strass, V.H., 2001. Sea ice transports in the Weddell Sea. J. Geophys. Res. 106, 9057–9073.
Hellmer, H.H., Kauker, F., Timmermann, R., 2009. Weddell Sea anomalies: excitation, propagation, and possible consequences. Geophys. Res. Lett. 36, L12605. doi:10.1029/2009GL038407.
Hellmer, H.H., Huhn, O., Gomis, D., Timmermann, R., 2010. On the freshening of the northwestern Weddell Sea continental shelf. Ocean Sci. Discuss. 7, 2013–2042. doi:10.5194/osd-7-2013-2010.
Heywood, K.J., Stevens, D.P., 2007. Meridional heat transport across the Antarctic Circumpolar Current by the Antarctic Bottom Water overturning cell. Geophys. Res. Lett. 34, L11610. doi:10.1029/2007GL030130.
Hoppema, M., Fahrbach, E., Schröder, M., Wisotzki, A., De Baar, H.J.W., 1995. Winter–summer differences of carbon dioxide and oxygen in the Weddell Sea surface layer. Mar. Chem. 51, 177–192.
Jacobs, S.S., Giulivi, C.F., Mele, P.A., 2002. Freshening of the Ross Sea during the late 20th century. Science 297, 386–389.
Kerr, R., Mata, M.M., Garcia, C.A.E., 2009. On the temporal variability of the Weddell Sea Deep Water masses. Antarct. Sci. 21, 383–400.
Klatt, O., Boebel, O., Fahrbach, E., 2007. A profiling float's sense of ice. J. Atmos. Oceanic Technol. 24, 1301–1308.
Melling, H., 1998. Sound scattering from sea ice: aspects relevant to ice-draft profiling by sonar. J. Atmos. Oceanic Technol. 15, 1023–1034.
Melling, H., Johnston, P.H., Riedel, D.A., 1995. Measurements of the topography of sea ice by moored subsea sonar. J. Atmos. Oceanic Technol. 12, 589–602.
Melling, H., Riedel, D.A., 1995. The underside topography of sea ice over the continental shelf of the Beaufort Sea in the winter of 1990. J. Geophys. Res. 100, 13641–13653.
Nicholls, K.W., Østerhus, S., Makinson, K., Gammelsrød, T., Fahrbach, E., 2009. Ice-ocean processes over the continental shelf of the southern Weddell Sea, Antarctica: a review. Rev. Geophys. 47, RG3003. doi:10.1029/2007RG000250.
Orsi, A.H., Johnson, G.C., Bullister, J.L., 1999. Circulation, mixing, and production of Antarctic Bottom Water. Prog. Oceanogr. 43, 55–109.
Owens, W.B., Wong, A.P.S., 2009. An improved calibration method for the drift of the conductivity sensor on autonomous CTD profiling floats by θ–S climatology. Deep-Sea Res. I 56, 450–457.
Park, Y.-H., Charriaud, E., Fieux, M., 1998. Thermohaline structure of the Antarctic Surface Water/Winter Water in the Indian sector of the Southern Ocean. J. Mar. Syst. 17, 5–23.
Rack, W., Rott, H., 2004. Pattern of retreat and disintegration of the Larsen B ice shelf, Antarctic Peninsula. Ann. Glaciol. 39, 505–510.
Rintoul, S.R., 2007. Rapid freshening of Antarctic Bottom Water formed in the Indian and Pacific Oceans. Geophys. Res. Lett. 34, L06606. doi:10.1029/2006GL028550.
Schlitzer, R., 2010. Ocean Data View. 〈http://odv.awi.de〉.
Silva, T.A.M., Bigg, G.R., Nicholls, K.W., 2006. Contribution of giant icebergs to the Southern Ocean freshwater flux. J. Geophys. Res. 111, C03004. doi:10.1029/2004JC002843.
Spreen, G., Kaleschke, L., Heygster, G., 2008. Sea ice remote sensing using AMSR-E 89 GHz channels. J. Geophys. Res., 10.1029/2005JC003384.
Strass, V.H., 1998. Measuring sea ice draft and coverage with moored upward looking sonars. Deep-Sea Res. I 45, 795–818.
Strass, V.H., Fahrbach, E., 1998. Temporal and regional variation of sea ice draft and coverage in the Weddell Sea obtained from upward looking sonars. In: Jeffries, M.O. (Ed.), Antarctic Sea Ice: Physical Processes, Interactions and Variability. Antarctic Research Series, vol. 74, pp. 123–139.
Thompson, D.W.J., Solomon, S., 2002. Interpretation of recent Southern Hemisphere climate change. Science 296, 895–899.
Walkden, G.J., Heywood, K.J., Nicholls, K.W., Abrahamsen, P., 2009. Freshwater transport at Fimbulisen, Antarctica. J. Geophys. Res. 114, C08014. doi:10.1029/2008JC005028.
Zwally, H.J., Yi, D., Kwok, R., Zhao, Y., 2008. ICESat measurements of sea ice freeboard and estimates of sea ice thickness in the Weddell Sea. J. Geophys. Res. 113, C02S15. doi:10.1029/2007JC004284.